AD-A130 431 THE NEED FOR AN EXPANDED DEFINITION OF GLISTENING SURFACE(U) ROME AIR DEVELOPMENT CENTER GRIFFISS AFB NY R J PAPA ET AL. OCT 82 RADC-TR-82-271 1/1

UNCLASSIFIED F/G 20/14 NL

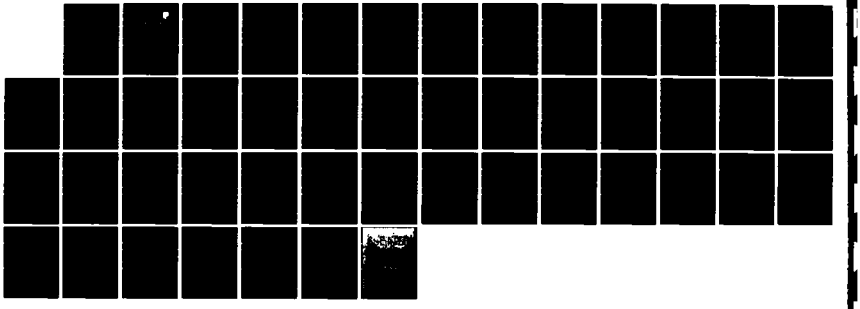

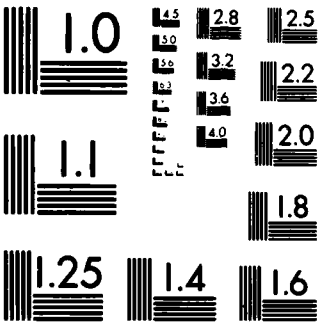

RADC-TR-82-271
In-House Report
October 1982

THE NEED FOR AN EXPANDED DEFINITION OF GLISTENING SURFACE

Robert J. Papa
John F. Lennon
Richard L. Taylor

APPROVED FOR PUBLIC RELEASE; DISTRIBUTION UNLIMITED

ROME AIR DEVELOPMENT CENTER
Air Force Systems Command
Griffiss Air Force Base, NY 13441

This report has been reviewed by the RADC Public Affairs Office (PA) and is releasable to the National Technical Information Service (NTIS). At NTIS it will be releasable to the general public, including foreign nations.

RADC-TR-82-271 has been reviewed and is approved for publication.

APPROVED: Philipp Blacksmith

PHILLIP BLACKSMITH
Chief, EM Techniques Branch
Electromagnetic Sciences Division

APPROVED: Allan C. Schell

ALLAN C. SCHELL
Chief, Electromagnetic Sciences Division

FOR THE COMMANDER: John P. Huss

JOHN P. HUSS
Acting Chief, Plans Office

If your address has changed or if you wish to be removed from the RADC mailing list, or if the addressee is no longer employed by your organization, please notify RADC (EECT), Hanscom AFB MA 01731. This will assist us in maintaining a current mailing list.

Do not return copies of this report unless contractual obligations or notices on a specific document requires that it be returned.

Unclassified

SECURITY CLASSIFICATION OF THIS PAGE (When Data Entered)

REPORT DOCUMENTATION PAGE		READ INSTRUCTIONS BEFORE COMPLETING FORM
1. REPORT NUMBER RADC-TR-82-271	2. GOVT ACCESSION NO. A130481	3. RECIPIENT'S CATALOG NUMBER 82-438
4. TITLE (and Subtitle) THE NEED FOR AN EXPANDED DEFINITION OF GLISTENING SURFACE		5. TYPE OF REPORT & PERIOD COVERED In-House Report 6. PERFORMING ORG. REPORT NUMBER
7. AUTHOR(s) Robert J. Papa John F. Lennon Richard L. Taylor		8. CONTRACT OR GRANT NUMBER(s)
9. PERFORMING ORGANIZATION NAME AND ADDRESS Electromagnetic Sciences Division (RADC/EEC) Hanscom AFB Massachusetts 01731		10. PROGRAM ELEMENT, PROJECT, TASK AREA & WORK UNIT NUMBERS 61102F 2305J407
11. CONTROLLING OFFICE NAME AND ADDRESS Electromagnetic Sciences Division (RADC/EEC) Hanscom AFB Massachusetts 01731		12. REPORT DATE October 1982 13. NUMBER OF PAGES 43
14. MONITORING AGENCY NAME & ADDRESS (if different from Controlling Office)		15. SECURITY CLASS. (of this report) Unclassified 15a. DECLASSIFICATION DOWNGRADING SCHEDULE

16. DISTRIBUTION STATEMENT (of this Report)

Approved for public release; distribution unlimited.

17. DISTRIBUTION STATEMENT (of the abstract entered in Block 20, if different from Report)

18. SUPPLEMENTARY NOTES

RADC Project Engineer: Robert J. Papa, RADC/EEC

19. KEY WORDS (Continue on reverse side if necessary and identify by block number)

Terrain
Rough surface scattering
Glistening surface

20. ABSTRACT (Continue on reverse side if necessary and identify by block number)

The first topic of this report is an analysis of the conditions under which the conventional definition of length of the glistening surface, as given by Beckmann and Spizzichino, is not valid. For a wide range of conditions, significant amounts of incoherent scattered power can be received from areas beyond the conventional length. A second topic is the investigation of the effect on angular tracking accuracy due to such scattering factors as shadowing, surface height distribution, standard deviation in surface height σ, surface correlation length l, unevenness and inhomogeneity of the terrain,

DD FORM 1473 EDITION OF 1 NOV 65 IS OBSOLETE

Unclassified

SECURITY CLASSIFICATION OF THIS PAGE (When Data Entered)

20. (Contd)

antenna heights, [illegible] interesting results have been observed. The amount of the non-coherent power not included in the coherent addition decreases rapidly, except for the case where both transmitter and receiver are very close to the surface. Next, a Gaussian surface height distribution generally results in less diffuse scattering than an exponential one. The trends seen in the results for scattering from the glistening surface do not differ for horizontal or vertical polarization, for Gaussian or exponential surface height distribution, or for different signal frequencies in the S-band to L-band regions. In an absolute sense, the results for vertical polarization indicate that there would be greater angular tracking accuracy for that case than for horizontal polarization, a result of particular interest for radar applications.

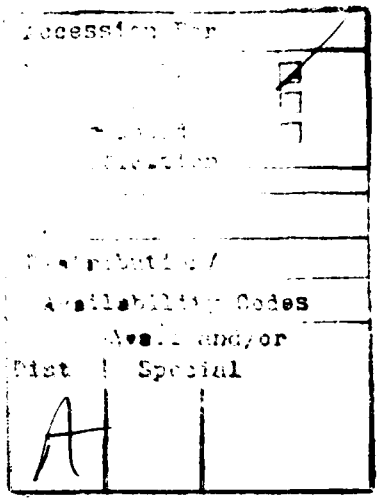

Contents

Illustrations

Illustrations

Tables

The Need for an Expanded Definition of Glistening Surface

I. INTRODUCTION

Electromagnetic signals scattered from rough terrain include contributions from clutter return and multipath return.[1,2] These two aspects can be described theoretically if properties of the terrain such as the probability density function (PDF) for the surface height distribution, the covariance matrix R, the variance in surface height,[2] and the complex dielectric constant characterizing the surface are known. The numerous theoretical models of EM wave scattering from rough surfaces[1,2,3,4,5] all relate the normalized cross section of terrain to the foregoing parameters of the rough surface.

1.1 Background

The problem of scattering from terrain is a primary interest at RADC/EEC. There have been a number of models developed which have represented the phenomena involved in the scattering in different ways. Two main elements common to all the techniques are the description of terrain features by the use of statistical estimation theory and the electromagnetic scattering formulation that incorporates the statistical results.

(Received for publication 2 January 1980)

(1)Due to the large number of references cited above, they will not be listed here. (See References, page 35.)

Extensive descriptions of the various statistical and electromagnetic models can be found in earlier reporting.[6,7] In those models we have used the concept of "glistening surface" (that part of the rough surface from which reflected waves can reach the receiver for a given position of the transmitter and receiver) as described by Beckmann and Spizzichino.[1] Their expressions for the length and width of the glistening surface were derived by making certain assumptions about the physical mechanisms occurring when EM waves are scattered from a rough surface. Some general discussion of the models will be outlined here; further details are presented in Appendix A. A computer program has been developed which has the capability of calculating the coherent (specular plus direct) and incoherent multipath power reaching a monopulse receiver from a beacon located over rough terrain. Discussions of coherence and the methods for calculating the coherent and incoherent power are given in Appendix A. The results that were obtained are discussed in terms of comparisons with test results at the Discrete Address Beacon System (DABS) site.[8] A geometrical representation of the experimental conditions is shown in Figure 1.

Bahar[9] has obtained very general expressions for the normalized cross sections (σ°) of rough surfaces using the full wave approach. He has shown that when the major contributions to the scattered fields come from regions of the rough surface around the stationary phase points, the full wave solutions reduce to the physical optics solutions. In our models, the expressions for σ° are based upon the physical optics approximations.

When the surface heights are normally distributed, the expression for σ° used in this study is one derived by Hagfors,[10] Barrick,[11] and Semenov.[12] When the surface heights are described more accurately by a bivariate exponential, then σ° is given by an expression derived in Ruck et al.[2] Two previous studies[13,14] have indicated that the surface heights for certain terrain are better described by multivariate probability density functions having bivariate exponential marginal densities. This result comes from the use of the hypothesis testing procedure (see Appendix A) developed to characterize height data.

Another important aspect is the inclusion of the effect of local shadowing. Sancer's[15] shadowing function is used for normally distributed surface heights. An extension of Brown's[4] work accounts for shadowing in the case of exponentially distributed surface heights.

(Due to the large number of references cited above, they will not be listed here. See References, page 35.)

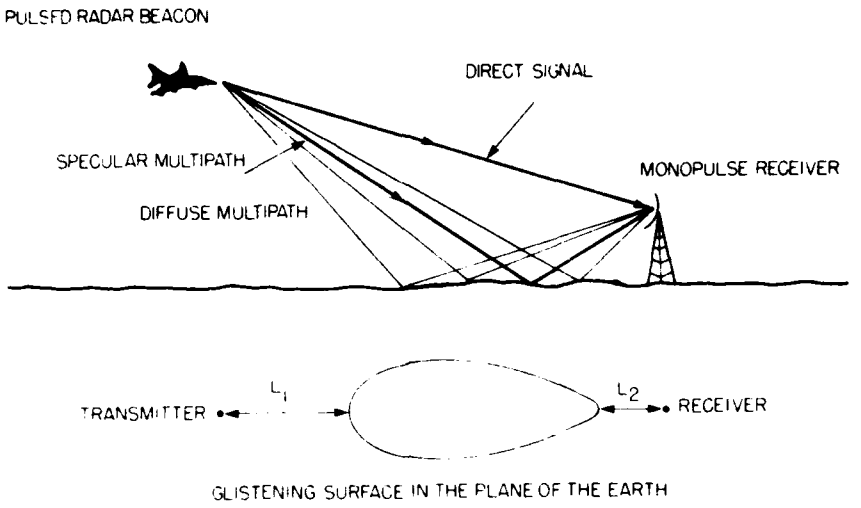

Figure 1. Specular and Diffuse Forward-Scatter From a Rough Surface and a Representation of the Glistening Surface

1.2 The Problem

In the previous studies, the use of the Beckmann-Spizzichino definition in the application of the models to the DABS test conditions resulted in underprediction of the azimuthal angle uncertainty σ_ψ and the associated diffuse power, particularly at short ranges. As a result we were led to an examination of the length definition for such conditions. As an alternative, we chose to consider the entire extent of the antenna separation as the surface contributing to the received diffuse power. The defining relations for the two surfaces of integration are the following (see Figure 1):

First there is the length as given by Beckmann and Spizzichino.[1] They determine the length by calculating the location of the two end points of the glistening surface. For a homogeneous surface, the distances from the end points to the transmitter and receiver (L_1, L_2) are based on the respective heights (H_T, H_A) and a roughness criterion (σ/T) where σ^2 is the surface height variance and T is the correlation length. Then,

$$L_1 = H_T \cot(2\beta_0)$$

$$L_2 = H_A \cot(2\beta_0) \qquad (1)$$

where

$$\tan \beta_o = 2\sigma/T .$$

In the extended length definition, the entire distance along the surface between the transmitter and receiver is included and, effectively, $L_1 = L_2 = 0$.

For both cases, Beckmann and Spizzichino's definition of width (W) of the glistening surface is used:

$$W = \frac{2X_1 X_2}{D} \left(\frac{H_A}{X_1} + \frac{H_T}{X_2} \right) \left[\tan^2 \beta_o - 0.25 \left(\frac{H_A}{X_1} - \frac{H_T}{X_2} \right)^2 \right]^{1/2} . \qquad (2)$$

Here,

D = total ground distance from transmitter to receiver,

X_1 = distance from transmitter to point on glistening surface,

X_2 = distance from receiver to point on glistening surface.

When the extended length was included in the model it was found that better agreement with the experimental data could be obtained with this version. The experimental data was taken by Lincoln Laboratory personnel[8] at the Discrete Address Beacon System (DABS) test site. The data used for comparison, boresight azimuthal pointing direction as a function of range, has been processed to remove the contribution associated with the fact that the mechanical and electrical boresight directions do not coincide. The boresight pointing direction data was divised into range bins and a local mean-azimuthal-pointing-direction was established for each bin. Then, the standard deviation about the local mean was calculated. This standard deviation represents the azimuthal angular uncertainty, σ_μ of their monopulse receiving antenna. (Following generally accepted usage, this report contains three similar symbols having distinct meanings. Care should be taken to distinguish σ, σ , and σ_μ.)

The angular uncertainty increases as the amount of diffuse multipath power entering the receiver increases. An expression relating σ_μ to the diffuse power scattered into the receiver is given in Appendix A. It includes contributions from noise in the system.

Figure 2 shows the diffuse power for the two theoretical models and the results based on the experiment. The terrain data base allows comparison only for ranges less than 60 km. The extended definition of the glistening surface provides better overall agreement with the experimental data, particularly for ranges R less than 45 km. For those ranges, the Beckmann and Spizzichino definition gives the result that the glistening surface does not exist and thus there is no diffuse power. The

overall behavior is more complicated than this and requires some additional comment. It should be noted that some additional cases where there is discrepancy have been found.[7] Those surfaces were uniform with given roughness levels. The effect of range definition in those cases is similar to that for the powerful conditions of the experimental data.

COMPARISON OF DIFFUSE POWER DATA AND RESULTS FROM THEORETICAL MODELS

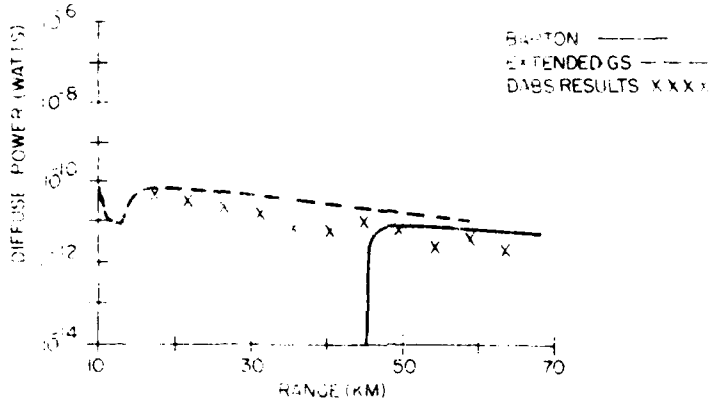

Figure 2. Comparison Between Usual Glistening Surface, Extended Glistening Surface, and DABS Data: Diffuse [illegible] Range

In all instances, the azimuthal error and diffuse power vanish for some [illegible] operations when the Beckmann-Spizzichino definition is used. This is [illegible] conditions. The glistening surface must be nonexistent for the Beckmann-Spizzichino model. Alternately, if the surface exists then the cross section [illegible] surfaces negligible. For $\sigma^2 = 0$ m^2 and $\sigma^2 = $ m^2, there is [illegible] values of the rms displacement exceed the correlation of the [illegible] the situation [illegible] with this [illegible] Figure shows the [illegible] set [illegible] location and [illegible] The [illegible] σ^2 [illegible] The [illegible] [illegible] [illegible]

[illegible] Barton, [illegible], and Fisher, [illegible] [illegible] [illegible] [illegible], Chapter [illegible].

significant σ^2 become narrower with peaks centered near the specular point location. When the region over which σ° is large is not included in the glistening surface, the result will be correspondingly small diffuse power contributions and angular errors. A further point is that even for sufficiently large σ^2 values, there are likely to be σ° contributions from the surface areas excluded by the Beckmann-Spizzichino L_1 and L_2 values.

These various findings provided the motivation for a study of the implications of using the conventional length definition and consideration of when it would not be satisfactory.

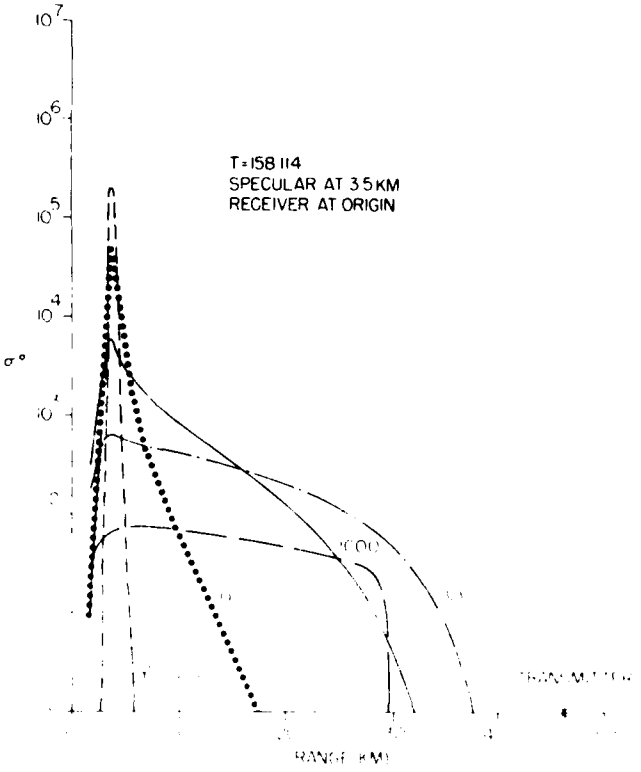

Figure 6. Variation of σ° Across the Antenna Beam Region, T = 158,114 s

1.3 Scope

The present study addresses a number of problems associated with the use of the conventional length definition and the specular point theory. In Section 2 we

For the purposes of this study we selected a set of nominal conditions which were used in the majority of cases. In these representative cases we consider homogeneous surfaces where the heights are assumed to have a bivariate exponential dependence. The surfaces are considered to be cultivated terrain with complex dielectric constant: 80 + j 9.0. For consistency with the nonuniform data base cases, these results are also terminated at a range of 55 km.

A wide range of results are presented. The first aspect is the consideration of the generality of the effects. Frequency, polarization, surface height distribution, and antenna pattern are all allowed to vary. The next topic is a parametric study illustrating the factors controlling the need for the extended length. Then, some specialized conditions are considered. Finally, the overall question is assessed and additional topics which will be investigated in the future are outlined.

2. GENERALITY OF THE RESULTS

Most of the cases treated in our main study involve conditions appropriate to the DABS experiment. In this first part of the report we will show that although the results were first obtained for those conditions, they are not limited to them and similar behavior can be found for a wide range of additional conditions.

In this section, the rough surface is considered to be homogeneous and the mean height $\bar{Z} = 0.0$. The height of the transmitter is 1200 m and the height of the receiver is 100 m, unless specified otherwise.

2.1 Surface Height Distribution Effects

The hypothesis testing procedures described in Appendix A were used to determine whether the terrain heights at the DABS test site more nearly fit either a bivariate Gaussian or exponential distribution function. The results of these tests indicated a better fit to the bivariate exponential distribution function. As a result, most of the investigations on the effect of extending the length of the glistening surface in this report are conducted for exponential distributions in surface heights. We first want to show that this assumption does not critically affect the results.

For exponentially distributed surface heights and for the Beckmann and Spizzichino definition of glistening surface, Figure 4 shows typical patterns for boresight pointing accuracy σ_ψ as the variance σ^2 is changed for a given ℓ. When the extended length definition of the glistening surface is used, the azimuthal uncertainty and diffuse power be more greater than the Beckmann and Spizzichino cases (see Figure 5b). [illegible] the effects of extending ℓ. Comparisons of Figure 6 with Figure 4 [illegible] that the effect of [illegible] is [illegible] for either definition [illegible]

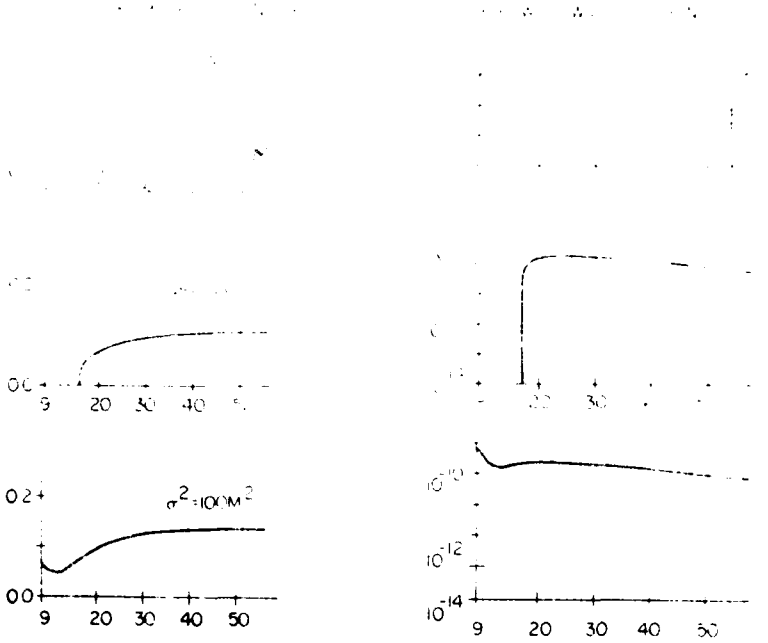

Figure 4. Diffuse Power and σ_θ Behavior for the Case of Beckmann and Spizzichino Length (BSL) Definition, T = 158, 114 m and No Shadowing

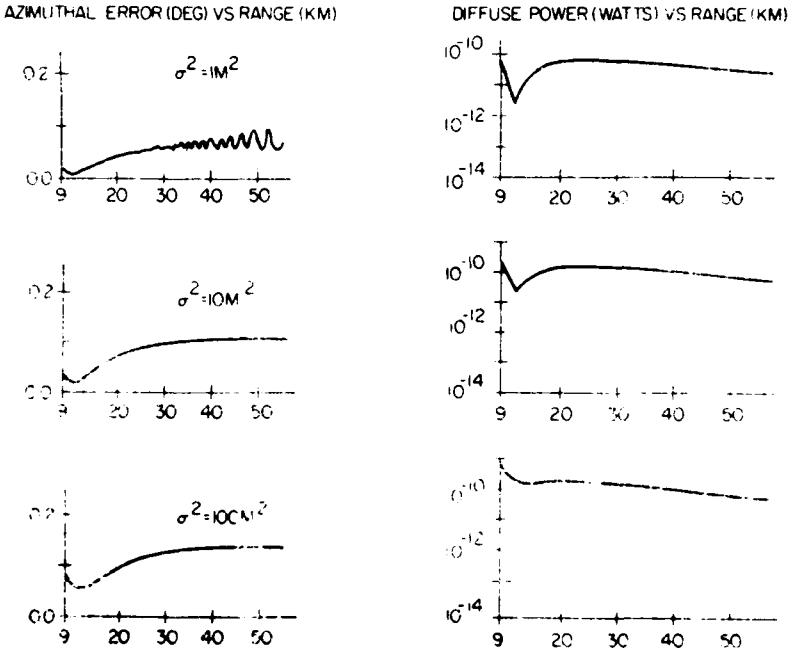

Figure 5. Diffuse Power and σ_θ Behavior for the Case of Extended Length (EL) Definition, T = 300 m and No Shadowing

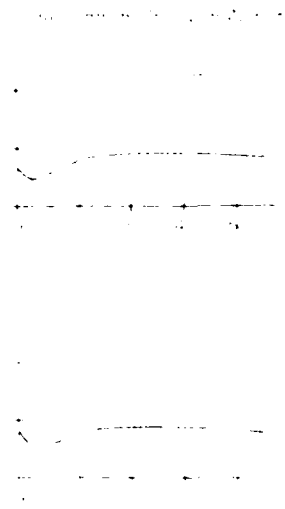

Figure 7. Comparison of Specular Power for the Gaussian Process, $\lambda = 500$ ft, $\sigma^2 = 2$

The above analyses have all assumed that the heights in the region are described by a Gaussian probability distribution function. No drastic differences would be seen, however, if the heights are considered to be described by a Gaussian autocorrelation. To illustrate this, some typical results are shown in Figure 7. The surface is flat, Power, $P_0 = 9.114$, and the antennas are at different heights. Comparison of these results with the corresponding exponential cases for the Beckmann-Spizzichino solution (see 4) and the extended length model (Figure 5) shows similar behavior for P_{DIFF} as a function of range. The bottom row of curves in Figure 7 is for $\sigma^2 = 10$ ft^2 the effect of shadowing is to cause a slight decrease in the specular power. This is again completely analogous to the case with exponentially distributed surface heights. To state briefly, the behavior is similar for long length lobes with the same values of σ^2 and ℓ resulting in less P_{DIFF} when the heights are assumed to be Gaussian distributed, rather than exponentially distributed.

2.2 Effects of Polarization

In the above analyses, it is generally assumed that the incident field electric vector is perpendicular to the plane of incidence of the rough surface. In this section the more general situation of an incident, plane wave whose electric vector is linearly polarized at some angle α relative to the plane of incidence of the rough surface is considered.

Qualitatively, it is clear that changing the polarization does not significantly affect the diffuse component of the coherent power at the receiver. Thus the diffuse power and σ_y can be determined from Beckmann's solution [1]. The left-hand curves in Figure 8 illustrate this result for both glistening surfaces in the case of a uniform surface, $\sigma^2 = 2$ ft^2 and $\lambda = 500$ ft, with the low-height antenna configuration.

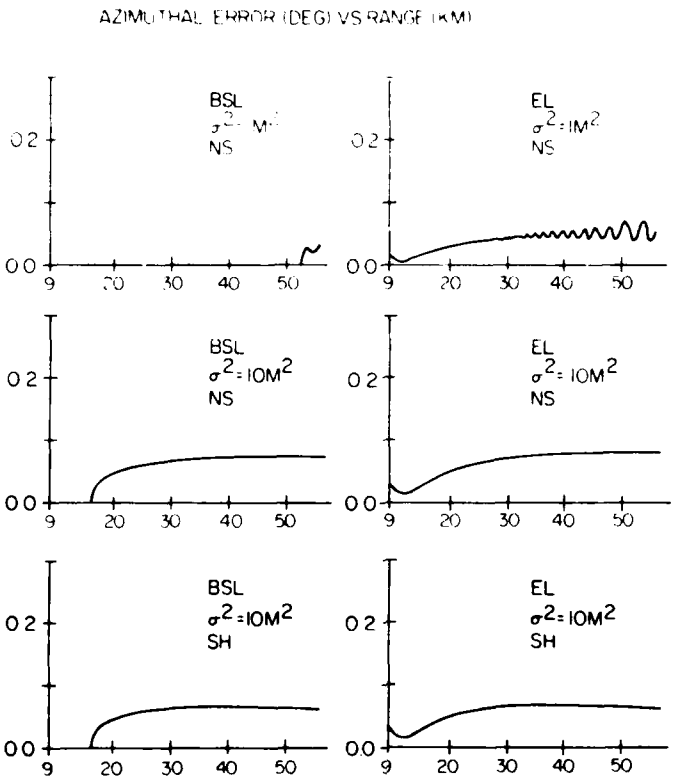

Figure 7. The Effect of Assuming Gaussian Surface Heights on σ_θ Behavior for Both Definitions, Uniform Surface, T = 158, 114 m

Another set of results for σ_θ is presented in Figure 9 (horizontal polarization) for the nonuniform surface (DABS data base) and various antenna height conditions. The equivalent vertical polarization results are shown in Figure 10. Although there is little effect when both antennas are close to the surface, there is some when both are at a distance above the surface. The most significant change occurs when the two antennas are at different heights. The extended length definition for that case is considerably more affected than is the Beckmann-Spizzichino case. The overall horizontal polarization behavior when the glistening surface is extended is analogous to the case for vertical polarization. Note that for all the antenna configurations there is less azimuthal angle error for vertical polarization than horizontal polarization.

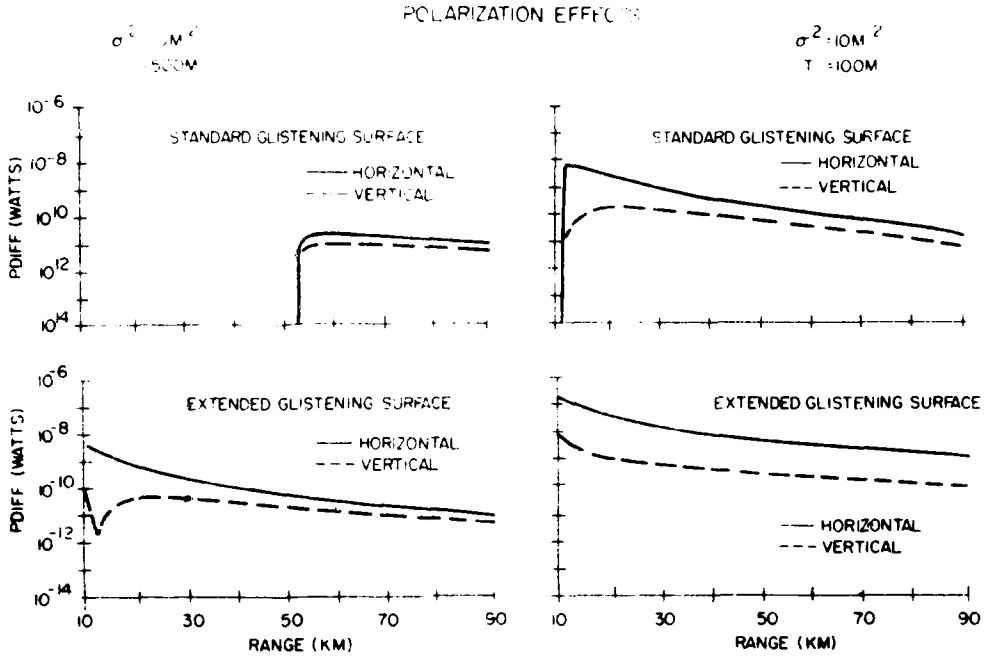

Figure 8. The Effect of Polarization on Diffuse Power Behavior for Both Definitions, σ^2 = 10 m^2, T = 100, 500 m with uniform surface and dual antenna heights

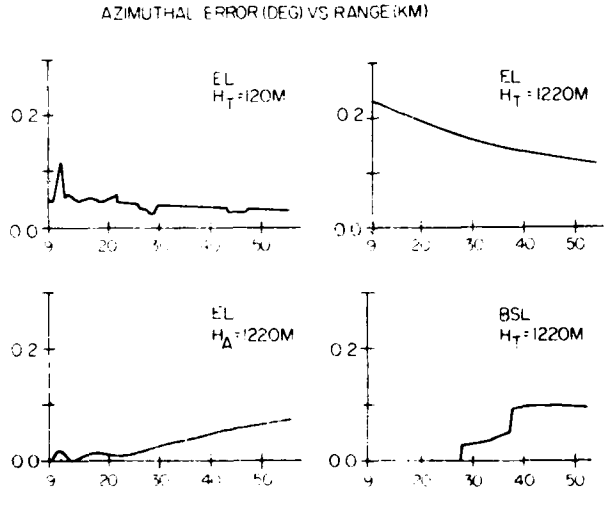

Figure 9. The Effect of Horizontal Polarization on σ_θ Behavior for Both Definitions, DABS Site Data, No Shadowing

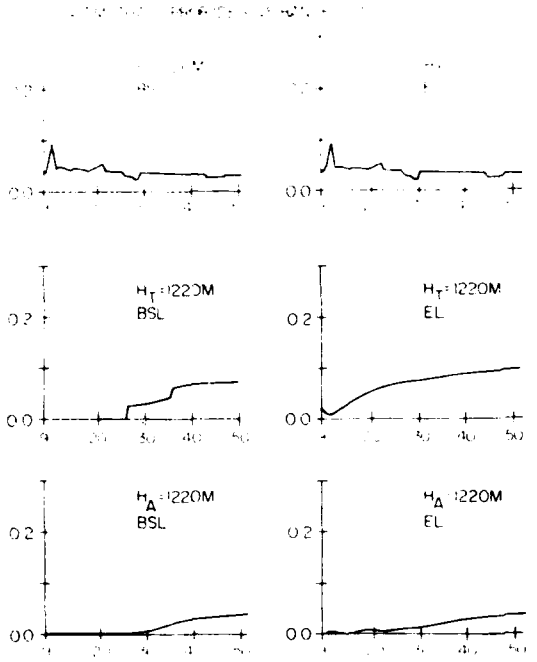

Figure 10. The Effect of Relative Antenna Heights on σ_θ Behavior for Vertical Polarization With Both Definitions and DABS Site Data

A decrease in azimuthal pointing error implies better tracking accuracy, and this aspect has been studied further. A computer program that simulates ground based radar detection and tracking of multiple targets was used to compare both polarizations in terms of relative tracking performance. In the simulation, an MTI radar is characterized as a one-dimensional rotating phased array with a three-pulse clutter cancellation system. The automatic tracker includes an α-β filter and has six-target maintenance capability. The environmental aspects include log-normally distributed ground clutter, Rayleigh distributed noise, specular multipath and terrain screening. Several track initiation and maintenance algorithms are employed. Monte Carlo techniques are used to calculate errors in range and angle estimation of each target's position.

The results of these simulations show that, in general, the MTI radar can more easily initiate and maintain track on multiple targets when the incident field is vertically polarized than when it is horizontally polarized. This is found to hold for various surface roughness parameters and several values of complex dielectric constant characterizing different classes of terrain.

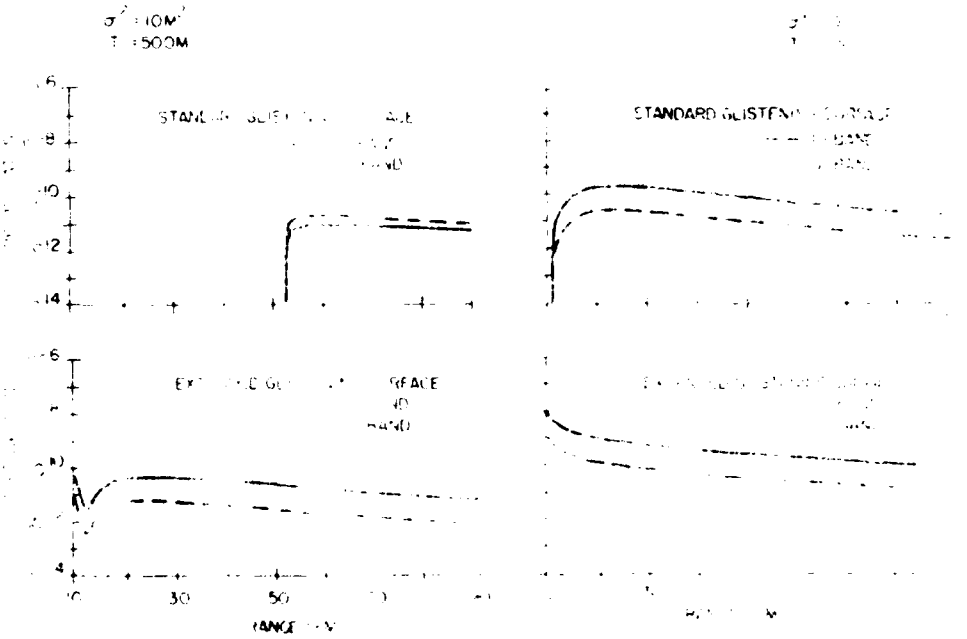
σ² = 10M²
R = 500M
STANDARD GLISTEN
-6
-8
-10
-12
-14
-6
30
50
RANGE

The left hand pair of graphs shows both glistening surface diffuse power results for the two frequencies, with $\sigma^2 = 10\ m^2$ and $T = 500\ m^2$. The right hand pair of figures shows both glistening surface diffuse power results for the two frequencies, with $\sigma^2 = 10\ m^2$ and $T = 100$ m. The general similarity is clear.

2.4 Antenna Pattern Effects

In Figure 12 we show the diffuse scattered power that results when two alternative elevation plane antenna patterns are substituted for the DABS configuration. The terrain is assumed to be a uniform surface and two levels of roughness are considered. T 500 m with $\sigma^2 = 10\ m^2$ and $\sigma^2 = 100\ m^2$. The figure shows the increase in diffuse power as a function of range when the glistening surface length is extended for both an isotropic elevation plane antenna pattern and a $\left(\frac{\sin x}{x}\right)$ pattern. It is clear that the results are equivalent for either pattern. The corresponding set of results for the DABS antenna pattern can be seen in Figures 13 and 14. In those figures the right hand side illustrations are the diffuse scattered power results for the conventional and the extended lengths respectively. Although these ranges terminate at 55 km, it is evident that the same results are present in this instance as occurred for the other two patterns.

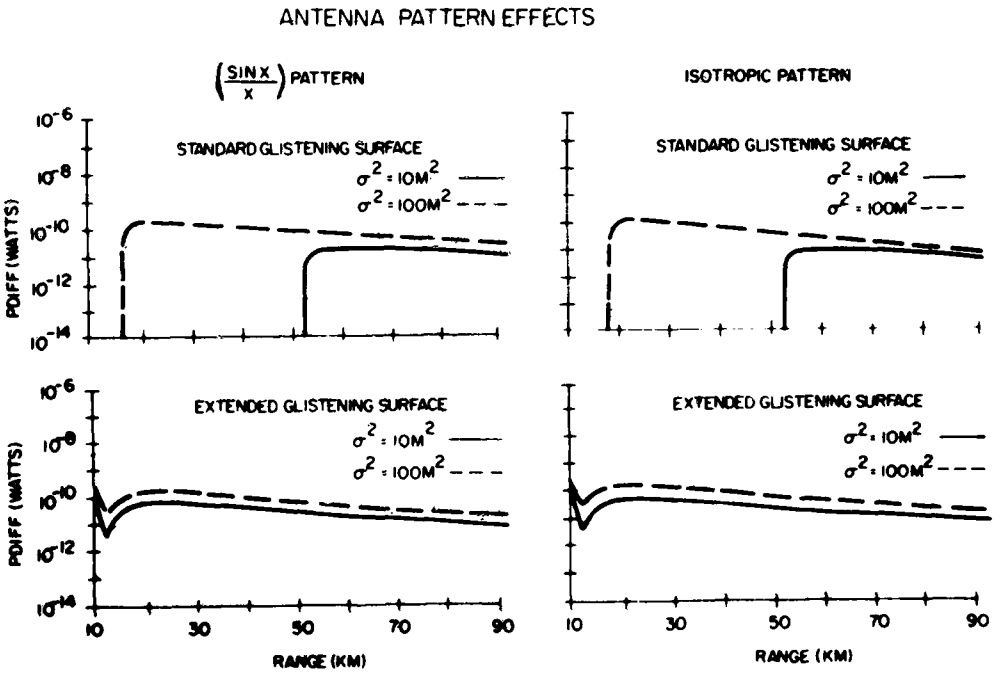

Figure 12. Antenna Pattern Effects for Both Definitions With T 500 m and $\sigma^2 = 10\ m^2$ and $\sigma^2 = 100\ m^2$

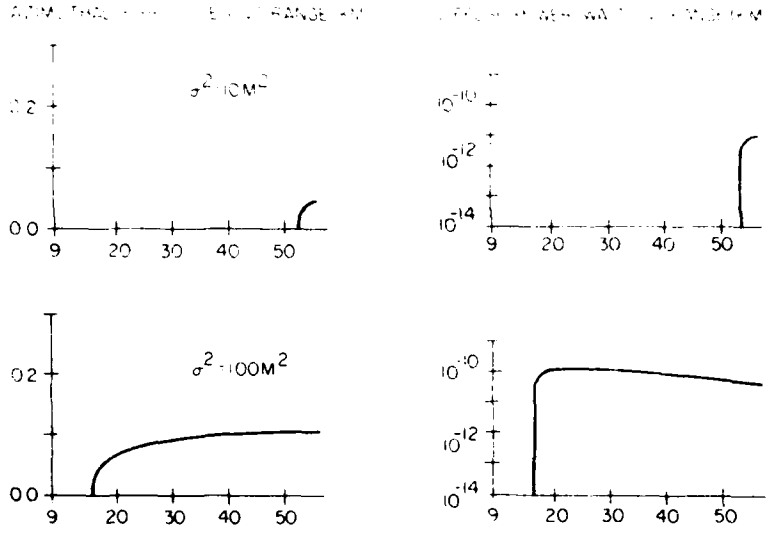

Figure 13. Diffuse Power and σ_θ Behavior for the Case of Beckmann and Spizzichino Length (BSL) Definition, T = 500 m and No Shadowing

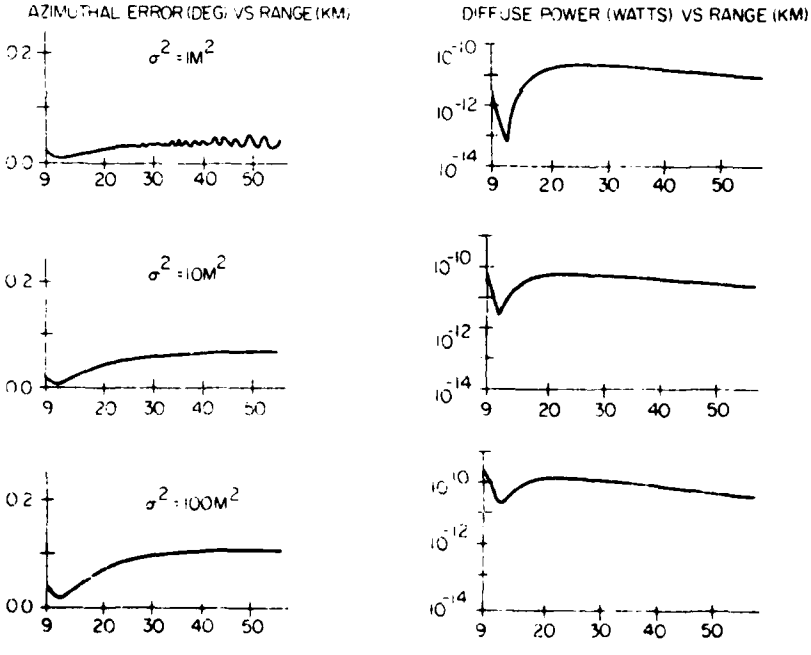

Figure 14. Diffuse Power and σ_θ Behavior for the Case of Extended Length (EL) Definition, T = 500 m and No Shadowing

3. PARAMETRIC STUDIES

In Section 2, we have shown that the usual definition of glistening surface length can result in diffuse power levels that are considerably different from the diffuse power at the receiver when the entire surface between the antennas is considered. The emphasis there was to show that this is not a localized result but rather quite general in terms of signal frequency, polarization, and type of surface height distribution. Now that this overall picture has been established, we will address how the two principal parameters in the Beckmann-Spizzichino formulation affect this outcome. These are the dependence of the results on the roughness factors, Γ and σ^2, as well as the dependence on the [illegible] angle. The type of results for the [illegible] are shown.

3.1 Results for Fixed Γ and Variable σ^2

[illegible]

To complete the discussion for T = 500 m, we want to consider whether there is any significant difference in the effect of local shadowing when the alternative definitions of the glistening surface length are used in the model. There is no effect on diffuse power or angular error when $\sigma^2 < 100\ m^2$ for either definition. For $\sigma^2 = 100\ m^2$, there was a slight decrease in σ_θ for R > 30 km. This can be seen by comparing Figure 15 with the corresponding cases in Figures 13 and 14. This is consistent with the expectation that the effects of shadowing would become more pronounced as σ^2 increases, since this corresponds to increasing the surface slopes. No significant difference in shadowing effects can be attributed to the use of the particular glistening surface definition.

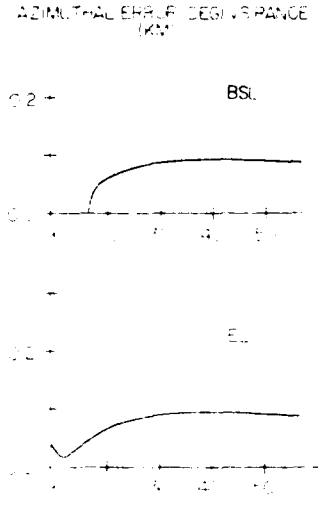

Figure 15. Comparison of Shadowing Effects for the Two Definitions, T = 500 m, $\sigma^2 = 100\ m^2$

For [illegible] and diffuse power with range for variable σ^2 values has been [illegible] one particular correlation length. We next want to consider the [illegible] σ^2 values at a second value, T = 158.114 m. This value was selected [illegible] comparisons of results for some ratios of σ/T that are equivalent to the [illegible] T = 500 m. This constant ratio comparison will be discussed in more de- [illegible] Section 4.2. The present discussion is just a general assessment of this [illegible] of results for both length definitions (note that these results have been [illegible] briefly in Section 2.1D).

For the Beckmann and Spizzichino definition, Figure 4 shows the typical in- [illegible] in $\sigma_{\theta\theta}$ and diffuse power with increasing σ^2. The shift in cutoff from 58 km [illegible] 15 km for example as σ^2 increases from $\sigma^2 = 1\ m^2$ to $\sigma^2 = 10\ m^2$. For $\sigma^2 = 100\ m^2$, [illegible] cutoff has appeared altogether.

Use of the extended length definition results in increasing the diffuse power and azimuthal uncertainty compared to the Beckmann and Spizzichino cases for $\sigma^2 = 1\ m^2$ and $\sigma^2 = 10\ m^2$ (see Figure 5). For those values, the apparent absence of angular uncertainty at some ranges is removed. The difference is most noticeable for $\sigma^2 = 1\ m^2$. There was no effect for antenna separations less than 55 km in the Beckmann-Spizzichino results while full integration shows that actually there is always angular error present. Of particular interest is the case for $\sigma^2 = 100\ m^2$. For that case, the two definitions have different results only for R < 18 km. For greater distances, the Beckmann and Spizzichino definition yields glistening surface lengths that encompass the significant σ° regions and generate results equivalent to the full integration cases.

We close the discussion on the behavior at T = 158.114 m by examining the effects of shadowing. Comparison of Figure 6 with Figures 4 and 5 confirms that again the effect of shadowing is the same for either definition of glistening surface length. For both definitions, the shadowing results in a decrease in σ_θ only for $\sigma^2 = 100\ m^2$ and then only for R > 20 km.

3.2 Results for Fixed σ^2 and Variable T

In this section the behavior of multipath effects are considered for fixed values of σ^2 with varying T with the same set of conditions as in Section 3.1.

Figure 16 shows the changes in σ_θ as a function of range for the Beckmann-Spizzichino definition when $\sigma^2 = 10\ m^2$ and T is increased from 1 m to 500 m. As T increases, beyond T = 100 m, a cutoff in σ_θ occurs which then appears at successively larger ranges. As T increases for the extended length definition (see Figure 17) there is a similar tendency towards a decrease in σ_θ at short ranges as T increases but no cutoff occurs at any T value. The analysis of the difference in results is similar to that introduced in Section 3.1.

The preceding discussion has been for the case where there is no shadowing in the model. Figure 18 introduces the effect of shadowing for $\sigma^2 = 10\ m^2$ and a range of T values. For T = 1 m and T = 10 m there is an appreciable shadowing effect. As T increases, the shadowing effect lessens and is significant mostly at longer ranges until for T = 500 m, there is no effect. The behavior is similar for both sets of glistening surface definition. This can be seen by comparing the two T = 10 m curves of Figure 18 with their respective unshadowed ones in Figures 16 and 17.

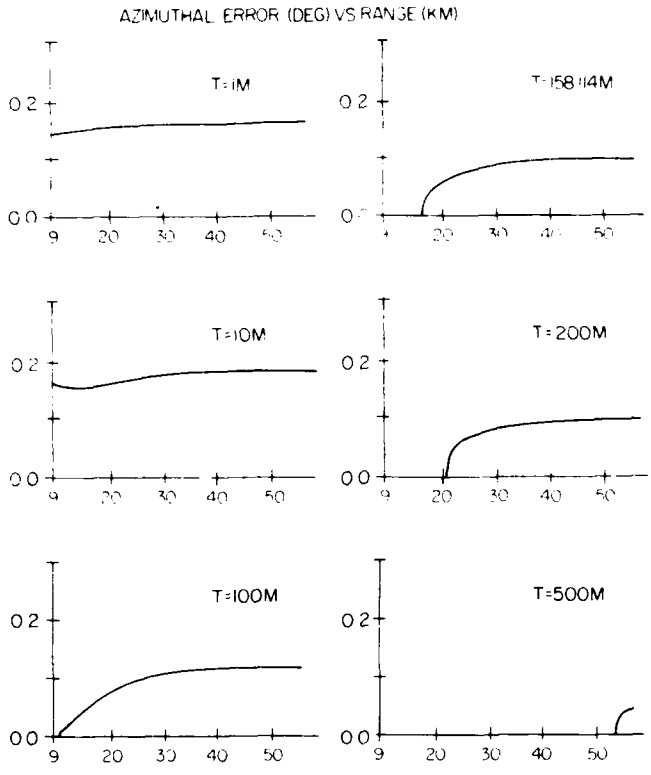

Figure 16. σ_θ Behavior for the Case of BSL Definition $\sigma^2 = 10\ m^2$, and No Shadowing

Computations also were performed for the case of $\sigma^2 = 1\ m^2$, and T varving from 10 m, to 158. 114 m. The behavior of σ_θ and diffuse power vs range is analogous to the case where σ^2 was fixed at 10 m^2 and T is increased from 100 m to 500 m. The coherent scattered power, though, is closer to flat surface conditions since σ^2 is less. Thus, the σ_θ curves have the corresponding oscillatory structure superimposed on the general variation. The general comment can be made that, for fixed σ^2, the effect of shadowing decreases as T increases since this corresponds to a decrease in surface slope (σ/T). Also, the shadowing is more pronounced at longer ranges which represent smaller grazing angles.

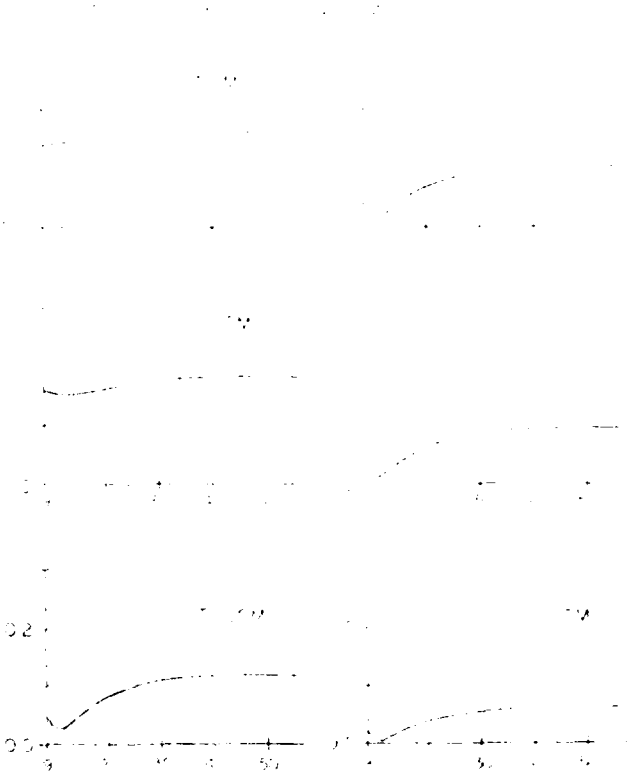

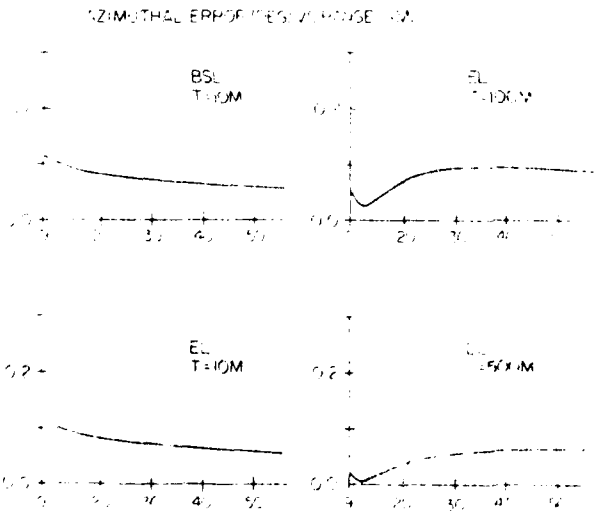
BSL
T=10M
EL
T=10M
EL
T=10M

4. FURTHER RESULTS

This section includes the effects on the EM wave scattering of varying the transmitting and receiving antenna heights, the effects of uniform vs nonuniform (real terrain) rough surfaces and the behavior of the sum pattern coherent power as a function of the system parameters.

4.1 Altitude of Antennas

4.1.1 A UNIFORM ROUGH SURFACE

In this section, it is assumed that the entire geological region is uniform, at zero mean height, that $\sigma^2 = 10\ m^2$, T = 500 m, that there is no shadowing and that the surface heights are exponentially distributed. In Figure 19, the effects of antenna height variations on σ_{ij} are shown for both length definitions. The first column of graphs in Figure 19 corresponds to the Beckmann-Spizzichino length case, and the second column corresponds to the extended length case.

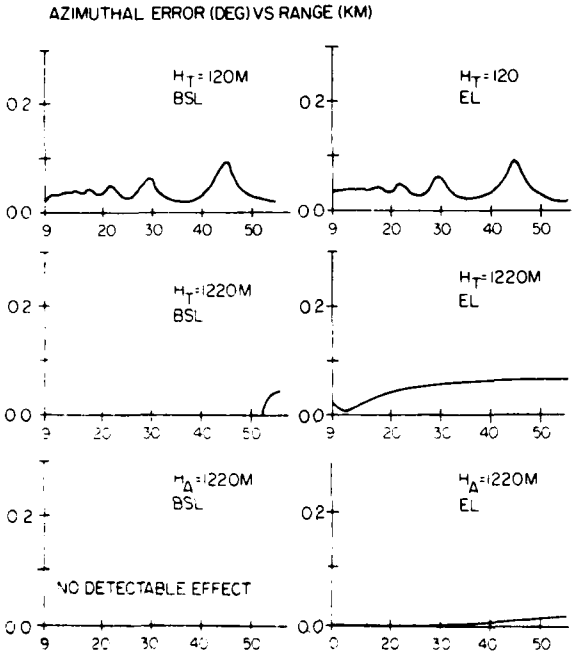

Figure 19. The Effect of Relative Antenna Heights on σ_{ij} Behavior for Both Definitions, Uniform Surface With T = 500 m and $\sigma^2 = 10\ m^2$

When each antenna [illegible] of σ_η as Beckmann definitions. [illegible] destructive interference between the [illegible] results in oscillations in the coherent component P_{COH} and corresponding oscillations in σ_η.

For the Beckmann-Spizzichino length definition, the glistening surface becomes smaller as H_T increases and the σ_η curve develops a cutoff. When both heights are increased, the length of the glistening surface approaches zero and there is no diffuse power nor σ_η at any range. For the extended length case, also, the diffuse power and σ_η decrease as either H_A or H_T is increased. This result may be attributable to a decrease in the width of the glistening surface.

Figure 20 shows the behavior of the diffuse power for the two surface types and different relative antenna heights. The extended length definition is used and no shadowing is present. The graphs on the right of Figure 20 show the uniform and nonuniform surface results for the dual antenna height condition. The results are quite similar. Those of the uniform surface are slightly higher for all ranges, with the greatest difference being at the vicinity of the dip at 12 km. This dip is due to local vanishing of the width of the glistening surface. For the low height case shown on the left, the two curves are again similar in behavior, with the uniform surface generating slightly more diffuse power. The curves no longer show any local minima. Lowering the antenna heights increases the value of P_{DIFF} at ranges less than 17 km, with a more rapid fall off with range beyond that point. This is not just due to changing the specular point since the uniform surface case shows similar behavior.

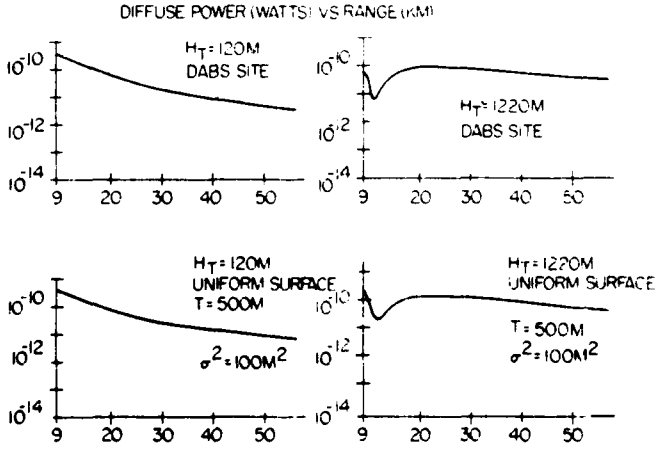

Figure 20. The Effect of Relative Antenna Heights on Diffuse Power for Both Surface Types, EL Definition and No Shadowing

4.1.2 NONUNIFORM TERRAIN

Figure 10 is completely analogous to Figure 19, except that the terrain characteristics correspond to an actual topographic data base (see Appendix A) instead of a uniform region.

An examination of Figure 10 shows that for both definitions there are abrupt oscillations in plots of σ_{γ} vs R when both antennas are near the surface. These variations are due to ray blockage (global shadowing) of the specularly reflected ray due to the unevenness of the terrain; the blocking results in abrupt variations in the coherent sum signal, and consequently in σ_{γ}. Consideration of the case where both antennas are close to the surface in Figure 19 might suggest that there should be several oscillations in σ_{γ} as R varies from 10 km to 55 km. However, this is not the case, because here the mean height of the terrain, $\overline{Z} \sim 60$ m, whereas for the uniform region (Figure 19) $\overline{Z} = 0$ m. It will be shown in Section 4.3 that, for $\overline{Z} = 60$ m, there are only one or two oscillations in P_{COH} between 10 km and 55 km.

Next we consider the dual antenna heights case. For the Beckmann-Spizzichino length case, the cutoff in σ_{γ} as H_T increases (see Figure 19) occurs for the nonuniform region results also. Similarly, extending the length of the glistening surface also results in a noticeable change in behavior of σ_{θ} for the dual heights case. Finally, for both antennas at a large distance above the surface, the extended length result for the average value of σ_{γ} vs R is approximately the same for the nonuniform surface as for the uniform region. This does not hold for the Beckmann-Spizzichino case since there is now a significant extent of ranges for which σ_{θ} is detectable.

4.1.3 THE EFFECTS OF SHADOWING

The topic here is the effect of shadowing for the various heights and surface conditions when both definitions of glistening surface are used. The top row of graphs in Figure 21 show the results for σ_{θ} with shadowing for the two types of surface with both antennas close to the ground. Since both definitions lead to similar effects for that case, only the extended length results are shown. Comparison of these two graphs with their corresponding unshadowed results in Figures 10 and 19, reveals only slight decreases due to the shadowing with a slightly greater effect for the nonuniform surface. The second row of graphs in Figure 21 show the result for σ_{θ} with shadowing for the nonuniform surface when both the antennas are at a large distance above the surface. Both definitions have been used. Comparison of these two results with the corresponding unshadowed cases in Figure 10, confirms that there is no noticeable contribution from shadowing under either definition for this antenna configuration.

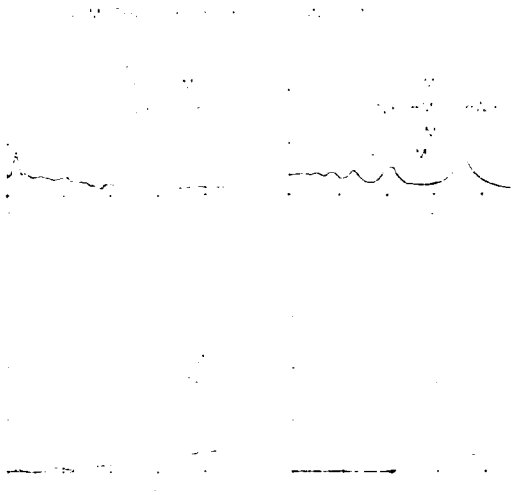

4.2 The Effects of the Ratio c/T

For [illegible] in Section 4.3 it will be shown that the coherent power depends on the ratio c/T. In Appendix A, it is shown that the mean power is a function of c/T. This corresponds to the fact that [illegible] the case $T \gg c$, [illegible] values [illegible] P_{DIFF} [illegible] c/T values. Figure 4.2 [illegible] P_{DIFF} [illegible] c/T values: $T = 158.73$ [illegible] $c = 3 \times 10^8$ m/s [illegible] $T = 500$ m with $c = 3 \times 10^8$ m/s [illegible] Figure 4.2 [illegible]

[illegible] of the [illegible] effects [illegible] behavior [illegible] c/T [illegible] c/T [illegible] values [illegible] a sharp peak near the second zero. As c/T increases, the power [illegible] magnitude. This [illegible] in location [illegible] the [illegible] of the [illegible] is [illegible] this [illegible] both [illegible]

4.3 Coherent Power Behavior

In this section, the behavior of the [illegible] power [illegible] the [illegible] of the [illegible] which [illegible] c/T [illegible] these [illegible] the [illegible] Figure 4.2 [illegible] the [illegible] P_{COH} [illegible] the

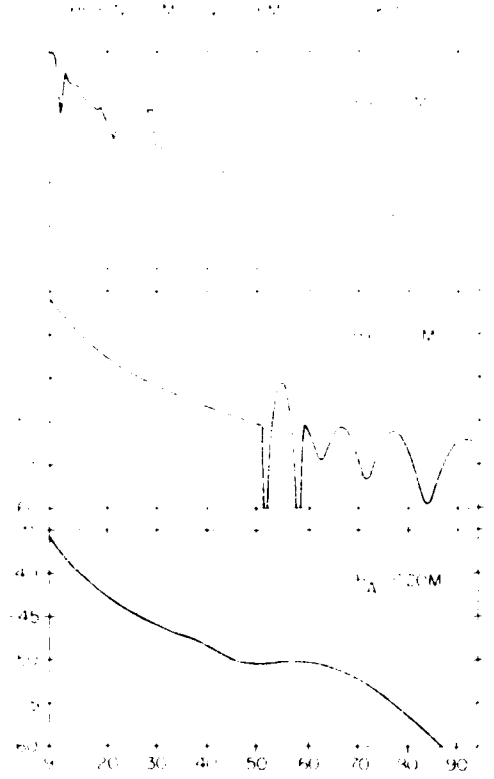

Figure 22. The Effect of Antenna Heights on Coherent Power Behavior for DABS Data

relative heights of the antennas are changed (DABS data base). In both equal height cases, the specular point and Fresnel zones tend to be centered between the two antennas while the dual height case results in specular regions close to the receiving antenna. Thus, the substantially different behavior beyond 50 km in that instance represents contributions to the coherent power from regions having a different (smoother) surface characterization from the other cases. In general, the three curves show relatively rough surface behavior. The significant difference being that for the low height case there are some ray blockage effects present and some possible multipath contributions at short ranges. This is supported by Figure 23. There, the $\bar{Z}$ = 60 m case shows typical behavior for a uniform flat surface with the antennas having the mean antenna height of the nonuniform case. The uniform surface removes the ray blockage effects for low antenna heights.

The remaining two curves of Figure 23 show the effect of surface height variance, σ^2, for the antennas close to the uniform surface with $\bar{Z}$ = 0 m. For σ^2 = 10 m^2 the coherent power shows large amplitude oscillations for R > 5 km. In contrast, for the same conditions, the dual height case results in the amplitude of the oscillations being small and occurring only at R > [illegible]. Even different

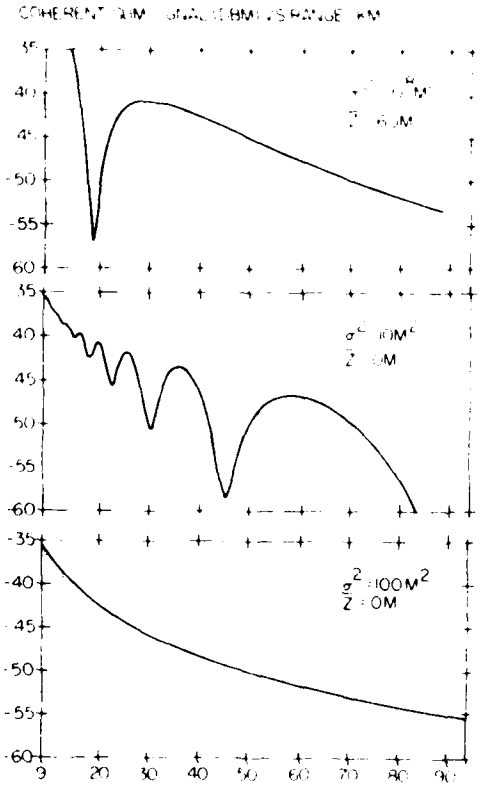

Figure 23. The Effect of $\bar{Z}$ and σ^2 on Coherent Power Behavior for a Uniform Surface, T = 500 m and Low Altitude Conditions

can be explained in terms of the fact that the amplitude of the coherent power is a complicated function of $\sigma \sin \theta/\lambda$ where λ is signal wavelength and $\sin \theta \approx (H_T - H_A)/R$. Then, for a given σ^2, a lower transmitter height increases the oscillation amplitudes and decreases the frequency of oscillation. Thus, only at large R values does the effective surface roughness ($\sigma \sin \theta/\lambda$) become small enough to cause oscillations in the dual height case, while the roughness is always sufficiently small in the low height case. Note that, beyond the R = 75 km point, no further oscillations are shown. This is due to the fact that the large amplitude and low frequency of the oscillations are incompatible with any additional plotting within the scale of the figure. In contrast, the curve for $\sigma^2 = 100\ m^2$ demonstrates that a sufficiently high variance in surface height preserves rough surface behavior even for the low height case.

5. SUMMARY AND CONCLUSIONS

To summarize the results of these studies, we start with discussions of the (σ, T) aspects. First, there is the behavior of σ° as a function of the surface distance from the receiver. It is found that, for both types of surface height distribution, graphs of σ° vs range, for a fixed transmitter location exhibit a peak at the specular point for small σ/T ratio (see Figure 3). This peak becomes less pronounced as the ratio (σ/T) becomes larger.

Next, for both exponentially and Gaussian distributed surface heights, the behavior of the diffuse power P_{DIFF} is a function only of the ratio (σ/T). The coherent power, P_{COH} is a function only of σ/λ. The azimuthal angle pointing error, σ_θ is a function of both P_{COH} and P_{DIFF}. For all altitudes, the effects of extending the length of the glistening surface on the behavior of P_{DIFF} and σ_θ vs R becomes more pronounced as the ratio σ/T becomes smaller. For small σ/T and both the dual height and high height antenna conditions, differences in P_{DIFF} of as much as 50 dB have been observed. For these cases, the Beckmann-Spizzichino definition of length may be such that the glistening surface does not include those regions which contribute appreciably to σ° (see Section 1 and Figure 3). In contrast to the P_{DIFF} behavior, as the ratio σ/T becomes smaller the effects of shadowing become less pronounced for the two surface height distributions.

The second area of discussion is that of the two glistening surface length definitions. Consider the effect of antenna height. For the Beckmann-Spizzichino length case, the length of the glistening surface becomes smaller as either the height of the antenna or the height of the transmitter is increased. Hence, using the extended length definitions changes the behavior of P_{DIFF} and σ_θ vs R for either the dual or high height conditions, while both definitions lead to equivalent results for the low height case.

Some length results do not depend on relative antenna heights or surface height distribution. First, the effects of extending the length of the glistening surface are more pronounced at short ranges than at long ranges. Second, extending the length of the glistening surface has no direct influence on the effects of shadowing. Also, for both length definitions, the effects of shadowing are more significant at longer ranges (smaller grazing angles).

Another distinct area is that of coherent power. For small and moderate values of σ, there are oscillations in P_{COH} vs R due to constructive and destructive interference between the direct ray and the specularly reflected ray. The oscillations in P_{COH} increase in amplitude and decrease in frequency as R increases. The result of this is that corresponding oscillations appear in the variation of σ_θ vs R if there is sufficient diffusely scattered power. A different coherent power phenomenon is

[illegible]

[illegible] height distribution. [illegible] scattered power, [illegible] the distribution of the surface points is assumed to be exponential [illegible] Rayleigh distribution. It should be recalled that [illegible] suggest that, for the nonuniform surface, the exponential distribution was more appropriate for the heights than the Rayleigh because of the agreement with the experimental results.

Although the form of the shadowing function for the two types of surface height distribution is different, these studies show that the effects of shadowing on P_{DIFF} and σ_ϕ in the two instances are qualitatively similar if all other parameters are equal. This similarity is also found in comparing the results of the two lengths of glistening surface.

The final area of discussion is the polarization of the signal. The effects of extending the length of the glistening surface on P_{DIFF} and σ_ϕ for horizontal polarization are completely analogous to those for vertical polarization. The studies lead to the general assertion that there is less diffusely scattered power and hence greater angular tracking accuracy when the incident field is vertically polarized. The results of the corroborative analysis of this aspect allow a further conclusion, that the effects of specular multipath for vertical polarization result in better tracking performance of an MTI radar system. This was found to be true at both L-band and S-band frequencies.

We have discussed the ranges of terrain statistics and system parameters for which the usual definition of glistening surface length may lead to significant underestimation of the diffuse scattered power and azimuthal pointing error. The magnitude of the effects associated with different radar or terrain characteristics has also been assessed. A number of additional aspects remain to be resolved. In the present study the width of the glistening surface was determined by the Beckmann-Spizzichino relation. Inasmuch as the length definition has proven to be inadequate, in many cases it may also be true that removing the width constraint may alter the results of the scattering. This can be explored by including an azimuthal variation in σ° in the calculations. Another aspect that will be investigated is the degree of sensitivity of the results to changes in the dielectric constant assigned to given surface features. This would correspond, for example, to consideration of the effect of moisture content in the soil.

References

1. Beckman, P., and Spizzichino, A. (1963) The Scattering of Electromagnetic Waves From Rough Surfaces, New York, Macmillan Co.
2. Ruck, G. T., Barrick, D. E., Stuart, W. D., and Krichbaum, C. K. (1970) Radar Cross Section Handbook, 2, New York, Plenum Press.
3. Long, M. W. (1975) Radar Reflectivity of L-band and Sea, Lexington, Books, Lexington, Massachusetts.
4. Brown, G. S. (1980) Shadowing by non-Gaussian random surfaces, IEEE Trans. Antennas Propagat. AP-28:788-790.
5. Peake, W. H. (1959) The Interaction of Electromagnetic Waves With Some Natural Surfaces, Antenna Laboratory, Ohio State University, Report No. 898-2.
6. Papa, R. J., and Lennon, J. F. (1980) Electromagnetic Scattering From Rough Surfaces Based on Statistical Characterization of the Terrain, presented at International Radio Science Symposium, (URSI), Quebec, Canada.
7. Papa, R. J., Lennon, J. F., and Taylor, R. L. (1980) Electromagnetic Wave Scattering From Rough Terrain, RADC-TR-80-300, AD A098939, Hanscom AFB, Massachusetts.
8. McGarty, T. P. (1975) The Statistical Characteristics of Diffuse Multipath and Its Effect on Antenna Performance, AD A009869.
9. Bahar, E. (1981) Scattering cross sections for random rough surfaces: Full wave analysis, Radio Science, 16:331-341.
10. Hagfors, T. (1964) Backscattering from an undulating surface with applications to radar returns from the moon, J. Geophys. Res. 68:3779-3784.
11. Barrick, D. E. (1968) Relation between slope probability density function and the physical optics integral in rough surface scattering, Proc. IEEE, 56:1728-1729.
12. Semenov, B. I. (1965) Scattering of electromagnetic waves from restricted portions of rough surfaces with finite conductivity, Radiotekh. i Elektron, 10:1952-1960.

13. Lennon, J. F., and Papa, R. J. (1980) Statistical Characterization of Rough Terrain, RADC-TR-80-9, AD A087746, Hanscom AFB, Massachusetts.

14. Papa, R. J., Lennon, J. F., and Taylor, R. L. (1980) Prediction of Electromagnetic Scattering for Rough Terrain Using Statistical Parameters Derived From Digitized Topographic Maps, RADC-TR-80-289, AD A094104, Hanscom AFB, Massachusetts.

15. Sancer, M. I. (1969) Shadow-corrected electromagnetic scattering from a randomly rough surface, IEEE Trans. Antennas Propagat. AP-17:577-585.

16. Papa, R. J., Lennon, J. F., and Taylor, R. L. (1981) An Improved Model for Scattering From Rough Terrain, presented at International Radio Sciences Symposium (URSI), Los Angeles, California.

17. Barton, D. K., and Ward, H. R. (1969) Handbook of Radar Measurement, Englewood Cliffs, New Jersey, Prentice-Hall, Inc.

Appendix A

Scattering Model

The results of this study were obtained from a sophisticated model describing the multipath effects associated with scattering of a signal by rough terrain. This model includes such factors as: (a) azimuthal and elevation power patterns of a monopulse receiver (see Figure A1); (b) the spatial nonuniformity of the rough earth; (c) nonuniformities in the glistening surface; (d) possible multiple specular reflection points due to unevenness in the surface; (e) the surface height distribution characterization and (f) both global and local shadowing effects.

The program normally uses system parameters associated with the L-band Discrete Address Beacon System to allow comparisons with experiment. These are defined in Table A1 and Figure A1. External inputs include the complex dielectric constant for each surface area, the coordinates of the monopulse receiver, the velocity and initial and final position of the aircraft containing the transmitter, and a parameter to control the effects of shadowing.

The description of the model may be divided into two major topics. These are the techniques required to assign appropriate statistical properties to the terrain and the specifics of the electromagnetic formulation. Each of these aspects requires some discussion.

There are several surface feature contributions in the model. Analyses of the scattering from rough surfaces consider the surface heights in the region as pairs of scattering elements and in most cases, including this study, assume that the height distribution can be described by either a bivariate Gaussian or exponential probability density. These two bivariate densities have the forms:

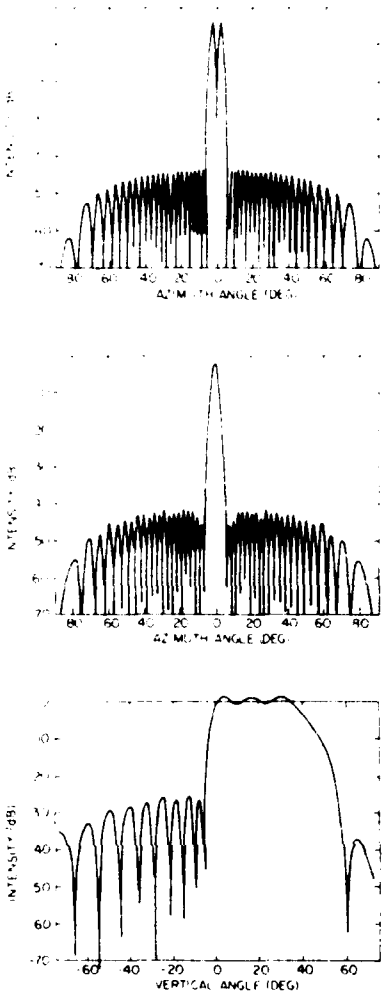

(Gaussian)

$$p(Z_1, Z_2) = \left(\frac{1}{2\pi\,\sigma^2\sqrt{1 - C^2}}\right)\exp\left[-\frac{(Z_1 - \mu_1)^2 - 2C(Z_1 - \mu_1)(Z_2 - \mu_2) + (Z_2 - \mu_2)^2}{2\,\sigma^2\,(1 - C^2)}\right]$$

(Exponential)

$$p(Z_1, Z_2) = \left(\frac{3}{2\pi\,\sigma^2\sqrt{1 - C^2}}\right)\exp\left[-\left\{\frac{(Z_1 - \mu_1)^2 - 2C(Z_1 - \mu_1)(Z_2 - \mu_2) + (Z_2 - \mu_2)^2}{\frac{1}{3}\,\sigma^2\,(1 - C^2)}\right\}^{1/2}\right]$$

Both forms have the same set of defining parameters, the mean height μ, the variance σ^2, and the correlation function C.

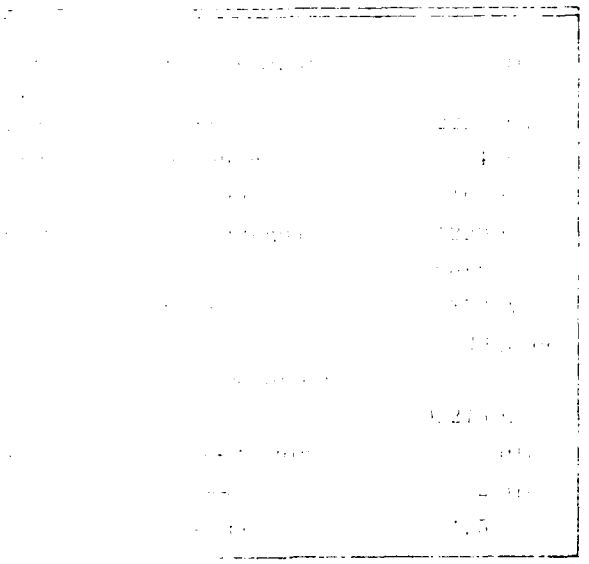

particular bivariate form, when
should be described by a higher order
required bivariate marginal density. A hypothesis
the two alternative multivariate densities that
joint values in the region simultaneously. Pure

simple alternative hypothesis test is equivalent to a minimum error probability criterion where it is equally likely that either density is the appropriate one.

For the comparison of the scattering theory with the experiment, these techniques had to be applied to the terrain at the eastern Massachusetts site. A data base of topographic elevations for this area is available at the Electromagnetic Compatibility Analysis Center (ECAC) in Annapolis, Maryland. This was prepared from digitized terrain maps supplied by the Defense Mapping Agency (DMA). The area of interest is divided into rectangular cells, each with sides of about 2 km. Each cell is further subdivided into a 10 by 10 grid of points. The statistical analysis is then applied to the individual cells.

The statistical data for each cell has been recorded on a computer tape for use with the program for the electromagnetic analysis. Each cell is represented by seven descriptors. The first two entries are the (x,y) coordinates for the center of the cell. Next is the geological code (dielectric constant) for the cell. (The predominant feature is woods; there are a number of cells containing clusters of lakes and ponds and a few town sites with associated cleared areas.) This is followed by the mean and variance of the heights in the cell and the estimated correlation length, T (the units of length are in meters). The final quantity is the result of the hypothesis test.

The trajectory of the beacon aircraft is incorporated into the computer program and at each range point for which a calculation is to be made the required cells and their descriptors are then identified. These results, or in the general case, the equivalent set of input parameters are then used in the electromagnetic analysis.

The calculation of the electromagnetic fields has two distinct elements. First, the total coherent electric field E_{COH} at the receiver is calculated using the sum pattern of the receiver antenna in the following expression:

$$E_{COH} = E_T \left[1 + \sum_j G_j(\theta_m) R_j \Gamma_{F_j} e^{ik\Delta R_j}\right] \qquad (A1)$$

where

E_T = direct path electric field at the receiver,

$G_j(\theta_m)$ = gain of receiver in direction of multipath ray, where θ_m is the angle between the direct ray and multipath ray,

R_j = attenuation factor affecting coherent reflected wave due to surface roughness,

Γ_{F_j} = complex Fresnel plane wave reflection coefficient,

k = $2\pi/\lambda$, and

ΔR = difference in path length between direct ray and reflected ray.

The summation over j represents all possible specular reflections (there may be more than one, due to unevenness in terrain). Here, coherence means there is a known phase relationship between the EM field leaving the transmitter and that reaching the receiver.

The next aspect is that of the diffuse power. The diffuse power in the monopulse difference channel is calculated from the expression

$$P_{DIFF} = \frac{P_T N_{LOSS} \lambda^2}{(4\pi)^3} \iint \left(\frac{G_{TR}^{AZ}(\phi_2)\, G_R^{AZ}(\phi_1)}{R_1^2 \quad R_2^2} \right) \cdot$$

$$\left(G_{TR}^{EL.}(\theta_1) G_R^{EL.}(\theta_2)\, \sigma^{-}(\theta_1, \theta_2) \right) \qquad \text{(A2)}$$

where

N_{LOSS} = system processing losses,

P_T = transmitted power,

λ = wavelength,

G_{TR}^{AZ} = gain (power) of transmitter in azimuth (isotropic pattern),

G_R^{AZ} = gain of receiver in azimuth (difference pattern, Figure A1),

$G_{TR}^{EL.}$ = gain of transmitter in elevation (isotropic pattern),

$G_R^{EL.}$ = gain of receiver in elevation (Figure A1),

θ_1 = elevation angle between boresight and point on glistening surface for transmitter,

θ_2 = elevation angle between boresight and point on glistening surface for receiver,

R_1 = range between transmitter and point on glistening surface,

R_2 = range between receiver and point on glistening surface,

dS = element of area of glistening surface which is illuminated by beacon,

ϕ_1 = azimuthal angle between boresight and point on glistening surface for receiver, and

ϕ_2 = azimuthal angle between boresight and point on glistening surface for transmitter.

The diffuse power integral contains an expression for the normalized average bistatic rough surface cross section, σ°, which comes from Beckmann et al.[7] The expressions derived by Beckmann are quite general and mighty complicated. In most situations, use simplified forms which follow from the assumption that the receiver is far from the transmitter so that the portion of the glistening surface that contributes to the diffuse multipath is a long, narrow strip extending between the transmitter and receiver. This assumption allows us to make the approximation that the azimuthal scattering angle $\phi_s \approx 0, 0$. This results in the relation:

$$\sigma^{\circ} \approx \sigma^{\circ}_{(\phi_s = 0)} S^2 \qquad (3)$$

where S = local shadowing function,

$$S = \left(\frac{1^2}{\sigma^2 \xi_z^2}\right) \exp\left[-\left(\frac{1^2}{4\sigma^2}\right)\left(\frac{\xi_x^2}{\xi_z^2}\right)\right]$$

for a Gaussian bivariate surface height probability density function and

$$S = \left(\frac{\sqrt{6}\,1^2}{\sigma^2 \xi_z^2}\right) \exp\left[-\left(\frac{\sqrt{6}\,1}{2\sigma}\right)\left(\left|\frac{\xi_x}{\xi_z}\right|\right)\right]$$

for an exponential surface height probability density function. The copolarized pairs of scattering elements in the matrix β_{pq} are given by

$$\beta_{vv} = \frac{(1 + \cos 2\alpha)\, R_{\perp}(\alpha)}{(\cos\theta_i + \cos\theta_s)} \quad \text{(vertical polarization)} \qquad (4)$$

with a similar expression for the horizontal-horizontal scattering matrix element β_{hh}. In the above expressions, the subscript $\perp$ refers to the E-field in the plane of incidence:

$$R_{\perp}(\alpha) = \frac{\epsilon_r \cos\alpha - \sqrt{\epsilon_r - \sin^2\alpha}}{\epsilon_r \cos\alpha + \sqrt{\epsilon_r - \sin^2\alpha}}$$

ϵ_r = the relative complex dielectric constant of the surface,

θ_i = angle of incidence (with respect to surface normal),

θ_s = angle of scattering (with respect to surface normal),

$\xi_x = \sin\theta_i - \sin\theta_s$,

$\xi_z = -\cos\theta_i - \cos\theta_s$,

The final aspect of the model is the azimuthal angle error. For this model, we assume that the spectral width of the diffuse multipath is narrow compared to the bandwidth of the receiver processor, and that both noise power and diffuse multipath power are Rayleigh distributed. For the conditions of the DABS System, the decorrelation time of the diffuse multipath power is of the order of 10^{-2} sec, and the interpulse period is of the order of 10^{-6} sec. Also, for the DABS experiment test site, the spectral width of the diffuse multipath power is of the order of 100 Hz, and the bandwidth of the receiver processor is about 5×10^4 Hz. This shows why even narrowband Doppler filtering cannot reduce the diffuse multipath power in the radar resolution cell containing the target. Under these conditions, the total amount of noiselike interference N_I in the radar resolution cell containing the signal is given by

$$N_I = P_{DIFF} + N_o \tag{A5}$$

where

N_o = Noise power from environment plus receiver.

The error, σ_θ, in azimuthal angle pointing accuracy is given by the expression of Barton and Ward:[17]

$$\sigma_\theta = \frac{\theta_B}{k_m \sqrt{2\,STIR}} \tag{A6}$$

where

θ_B = azimuthal beamwidth,

STIR = P_{COH}/N_I = signal to interference ratio in the difference channel,

P_{COH} = coherent power in sum channel,

k_m = normalized pattern slope.

---

[17] Barton, D.K., and Ward, H.R. (1969) Handbook of Radar Measurement, Englewood Cliffs, New Jersey, Prentice-Hall, Inc.

MISSION
of
Rome Air Development Center

RADC plans and executes research, development, test and selected acquisition programs in support of Command, Control Communications and Intelligence (C^3I) activities. Technical and engineering support within areas of technical competence is provided to ESD Program Offices (POs) and other ESD elements. The principal technical mission areas are communications, electromagnetic guidance and control, surveillance of ground and aerospace objects, intelligence data collection and handling, information system technology, ionospheric propagation, solid state sciences, microwave physics and electronic reliability, maintainability and compatibility.

Printed by
United States Air Force
Hanscom AFB, Mass. 01731

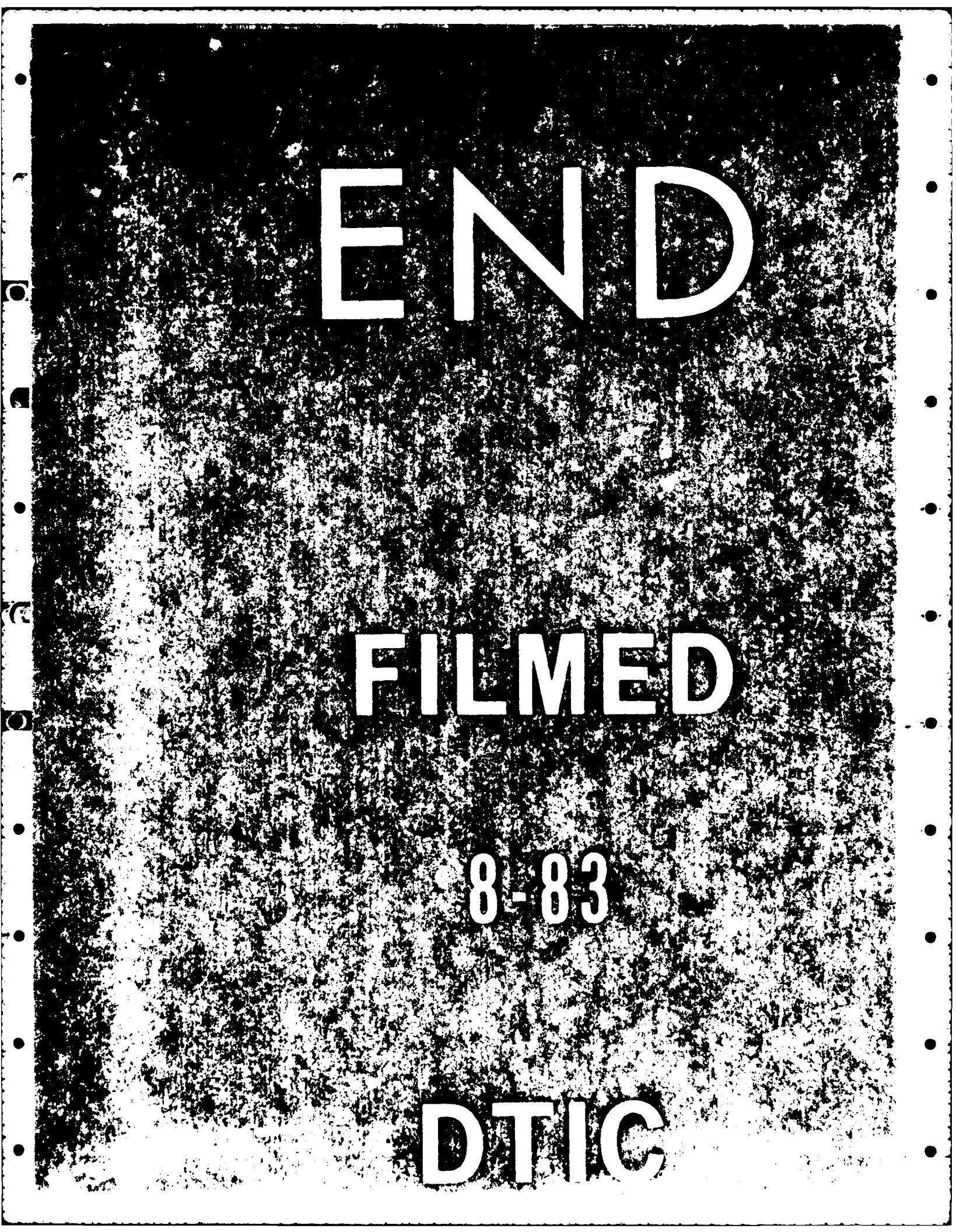
END
FILMED
8-83
DTIC